Anisotropic finite elements for the Stokes problem: a-posteriori error estimator and adaptive mesh

Maharavo Randrianarivony

Fakultät für Informatik
Technische Universität Chemnitz
Strasse der Nationen 62
D-09107 Chemnitz
GERMANY
maharavo@informatik.tu-chemnitz.de

Abstract

We propose an a-posteriori error estimator for the Stokes problem using the Crouzeix-Raviart/$\mathbf{P}_0$ pair. Its efficiency and reliability on highly stretched meshes are investigated. The analysis is based on hierarchical space splitting whose main ingredients are the strengthened Cauchy-Schwarz inequality and the saturation assumption. We give a theoretical proof of a method to enrich the Crouzeix-Raviart element so that the strengthened Cauchy constant is always bounded away from unity independently of the aspect ratio. An anisotropic self-adaptive mesh refinement approach for which the saturation assumption is valid will be described. Our theory is confirmed by corroborative numerical tests which include an internal layer, a boundary layer, a re-entrant corner and a crack simulation. A comparison of the exact error and the a-posteriori one with respect to the aspect ratio will be demonstrated.

Key words:
anisotropic mesh, Stokes problem, strengthened Cauchy, error estimator, adaptive mesh.

1 Introduction

In many practical situations, the solution to a partial differential equation has some preferred orientation. That is, it changes considerably fast toward certain directions. That is exemplified by problems presenting boundary or internal layers. Anisotropic meshes which contain thin and stretched elements

have been demonstrated to be suitable for solving such problems (See among many others [4,6,29,9,25,17]) .

In this document, we will focus mainly on the Stokes problem in two dimensions. It is a well known fact ([20]) that the inf-sup condition (also widely known as LBB-condition) guarantees the convergence of the FE-discretization. The stability of a velocity-pressure pair depends on whether its inf-sup constant is bounded away from zero. In contrast to several other velocity-pressure pairs ([30,7]) , the Crouzeix-Raviart/ $\mathbf{P}_0$, which we will use throughout this paper, is known to be unconditionally stable on any anisotropic mesh (see [5,2]) .

The objective of this paper is the investigation of a-posteriori error estimator for the Crouzeix-Raviart/ $\mathbf{P}_0$ pair on anisotropic grids. Further, we aim at using that estimator to construct an automatic self-adaptive (see [32,13,31] and the reference there) mesh refinement algorithm which starts from a coarse mesh. Basically, a-posteriori error estimators permit to evaluate the finite element errors without knowing the exact solution. That feature makes it possible to dynamically identify regions where one should have further refinements if the error there is too large. Therefore adaptive refinements are mainly based on the quality of a-posteriori error estimators.

Lots of related works have already been done in this topic. For isotropic grids, many different a-posteriori error estimators have been already proposed for the Stokes problem (see [33,34,3,22] and the references there). In the context of anisotropic meshes, there are already a variety of a-posteriori error estimators for Poisson and reaction-diffusion problems ([25,15,24,23]). For the Stokes equation, a recent article ([14]) by Creusé, Kunert and Nicaise presents a survey on the residual based error estimator on anisotropic grids. An interesting a-posteriori error estimator for two and three dimensions as well as an anisotropic adaptive mesh refinement are also detailed in [31].

In the present document, we propose an a-posteriori error estimator which is based on a hierarchical space enrichment whose major ingredients are the strengthened Cauchy-Schwarz inequality and the saturation assumption. We demonstrate a method to enrich the Crouzeix-Raviart element so that the strengthened Cauchy constant is always strictly smaller than the unity independently of the aspect ratio. We will show also an anisotropic mesh refinement technique which starts from a coarse and isotropic mesh and which keeps the saturation assumption valid.

The structure of the paper is as follows. In section 2, we introduce various definitions and notations. Section 3 treats exclusively the strengthened Cauchy-Schwarz inequality for the Crouzeix-Raviart element on stretched grids. We detail the a-posteriori error estimator in section 4. In the last section, we pro-

pose an anisotropic mesh refinement strategy. We analyze the performance of the investigated a-posteriori error estimator on four different problems: an internal layer, a boundary layer, a re-entrant corner and a crack problem. Additionally, we want to make a closer survey of the saturation assumption based on the proposed mesh refinement strategy. In all those tests, the expressions of the exact solutions are explicitly known so that we can make a clear comparison between the exact error and the a-posteriori estimated error.

2 Problem setting and notations

2.1 The Stokes problem

Let Ω be a polyhedral domain with Lipschitz boundary. The Stokes problem consists of searching for the velocity $\vec{u} = (u_1, u_2) \in V := H_0^1(\Omega)^2$ and the pressure $p \in Q := L_0^2(\Omega)$ such that

$$\begin{cases} (\nabla \vec{u}, \nabla \vec{v}) - (\operatorname{div} \vec{v}, p) = (\vec{f}, \vec{v}), & \forall \vec{v} \in V \\ (\operatorname{div} \vec{u}, q) = 0 & \forall q \in Q \text{ , where} \end{cases} \tag{1}$$

$$H_0^1(\Omega) := \left\{ v \in H^1(\Omega) : \ v = 0 \quad \text{on} \quad \partial\Omega \right\} \ , \tag{2}$$

$$L_0^2(\Omega) := \left\{ q \in L^2(\Omega) : \int_\Omega q = 0 \right\} \ . \tag{3}$$

2.2 Anisotropic mesh

Definition 1 An anisotropic mesh $\mathbf{T}_h$ is a set of disjoint triangles such that

$$\overline{\Omega} = \bigcup_{T \in \mathbf{T}_h} \overline{T}, \quad \text{and} \tag{4}$$

every edge of any element $T_i \in \mathbf{T}_h$ is *either* a part of the boundary $\partial\Omega$ *or* an edge of another element T_j of $\mathbf{T}_h$.

Remark 2 *For a triangle T, we denote*

$$h(T) := \operatorname{diam}(T) = \sup\{ \|\vec{x} - \vec{y}\|_{\mathbb{R}^2}, \ \vec{x}, \vec{y} \in T \} \, ,$$

$\rho(T) := \textit{supremum of the diameters of all balls contained in} T\,,$
$\sigma(T) := h(T)/\rho(T) = \textit{aspect ratio of}\, T\,.$

We will denote by $\partial\mathbf{T}_h$ *the set of all edges of elements in the mesh* $\mathbf{T}_h$ *and the aspect ratio of the mesh* $\mathbf{T}_h$ *is defined by*

$$\sigma_h := \max_{T\in\mathbf{T}_h} \sigma(T).$$

2.3 Crouzeix-Raviart/$\mathbf{P}_0$ *pair*

We approximate the velocity and the pressure in the following discrete spaces

$$V_h := \left\{ \vec{v}_h \in L^2(\Omega)^2 :\ \vec{v}_h|_T \in (P_1)^2\, \forall\, T \in \mathbf{T}_h \text{ and } \int_F [\vec{v}_h] = 0\ \forall F \in \partial\mathbf{T}_h \right\} \tag{5}$$

$$Q_h := \left\{ q_h \in L^2_0(\Omega) :\ q_h|_T \in P_0 \quad \forall\, T \in \mathbf{T}_h \right\}, \tag{6}$$

where $[\vec{v}_h]$ stands for the jump of $\vec{v}_h$ across the edge F if F is an internal edge, and it is equal to $\vec{v}_h$ itself if F is a boundary edge. For all $\vec{u}, \vec{v} \in V_h$ and $q \in Q_h$, we define

$$a_T(\vec{u},\vec{v}) := \sum_{j=1}^{2} \int_T \mathbf{grad}\, u_j \cdot \mathbf{grad}\, v_j\,, \quad b_T(\vec{v}, q) := \int_T q \,\mathrm{div}\, \vec{v}\,, \text{ and}$$

$$a_h(\vec{u},\vec{v}) := \sum_{T\in\mathbf{T}_h} a_T(\vec{u},\vec{v})\,, \quad b_h(\vec{v}, q) := \sum_{T\in\mathbf{T}_h} b_T(\vec{v}, q)\,.$$

The discrete problem deals with finding $\vec{u}_h \in V_h$ and $p_h \in Q_h$ such that

$$\begin{cases} a_h(\vec{u}_h,\vec{v}_h) - b_h(\vec{v}_h, p_h) = (\vec{f},\vec{v}_h), & \forall\, \vec{v}_h \in V_h \\ b_h(\vec{u}_h, q_h) = 0 & \forall\, q_h \in Q_h\,. \end{cases} \tag{7}$$

Let us introduce the broken Sobolev space

$$\mathbb{H} := \left\{ u \in L^2(\Omega) :\ u|_T \in H^1(T)\ \ \forall T \in \mathbf{T}_h \right\}.$$

The exact velocity and the pressure errors are respectively

$$\vec{u}_{\text{err}} := \vec{u} - \vec{u}_h \in \mathbb{H}^2 \tag{8}$$

$$p_{\text{err}} := p - p_h \in Q\,. \tag{9}$$

We will need the following scalar product and its corresponding energy norm later on

$$\langle \vec{u}, \vec{v} \rangle := a_h(\vec{u}, \vec{v}), \qquad |||\vec{u}||| := \langle \vec{u}, \vec{u} \rangle^{1/2} . \tag{10}$$

2.4 Simplification of the errors

Our idea is to avoid the evaluation of $\vec{u}_{\rm err}$ and $p_{\rm err}$ directly. Rather, we will first reduce these errors into a single error with a Poisson problem.

Lemma 3 Let $\vec{E} \in \mathbb{H}^2$ be the solution of

$$a_h(\vec{E}, \vec{v}) = a_h(\vec{u}_{\rm err}, \vec{v}) - b_h(\vec{v}, p_{\rm err}) \quad \forall\, \vec{v} \in \mathbb{H}^2 , \tag{11}$$

then

$$C_1 |||\vec{E}|||^2 \le |||\vec{u}_{\rm err}|||^2 + \|p_{\rm err}\|_0^2 \le C_2 |||\vec{E}|||^2 ,$$

where the constants C_1 and C_2 are independent of h and the aspect ratio σ_h of the mesh $\mathbf{T}_h$. C_1 and C_2 depend exclusively on Ω.

PROOF. This is proved in a very similar way as Theorem 1.1. of [3]. □

3 Strengthened Cauchy-Schwarz inequality

We propose in this section a way to enrich the Crouzeix-Raviart element on anisotropic meshes. Let T be an arbitrary triangle and $k = 2, 3$. Denote by $a_1,\ a_2, a_3$ the midpoints of its edges and by ϕ_i, $i = 1, 2, 3$ the linear polynomials in T for which $\phi_i(a_j) = \delta_{ij} \quad i,\ j = 1, 2, 3$. We refine T into k^2 similar triangles and denote by b_j ($j = 1, 2, 3$ for $k = 2$ and $j = 1, ..., 7$ for $k = 3$) the nodes which do not coincide with the apices of T (see Fig. 1). Finally let ψ_j be the piecewise linear nodal basis functions at b_j. The spaces spanned by ϕ_i and ψ_j are denoted by $V(T)$ and $Z(T)$ respectively. For scalar valued functions $u, v \in H^1(T)$, we define the following local entities

$$\langle u, v \rangle_T := \int_T \mathbf{grad}\, u \cdot \mathbf{grad}\, v \quad \text{and} \quad |u|_{1,T} := \langle u, u \rangle_T^{1/2}. \tag{12}$$

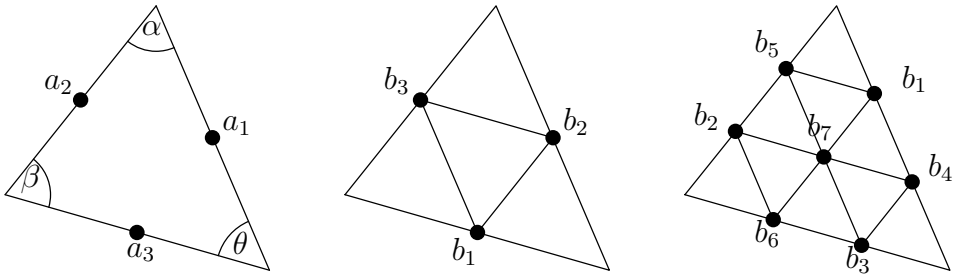

Fig. 1. Initial triangle; Refinement for $k = 2$; Refinement for $k = 3$

Theorem 4 Let T be a triangle. There exists a constant $\gamma \in [0, 1)$ which is independent of $\sigma(T)$, meas(T), $h(T)$ and $\rho(T)$ such that

$$\langle u, v\rangle_T \leq \gamma |u|_{1,T}.|v|_{1,T} \quad \forall u \in V(T),\ \forall v \in Z(T).$$

PROOF. The case $k = 2$ is already implicitly proved in [27] where $\gamma^2 = 3/4$, we only need to show it for $k = 3$. We should demonstrate that

$$\gamma := \sup_{u\in V(T)} \sup_{v\in Z(T)} \frac{\langle u, v\rangle_T}{|u|_{1,T}|v|_{1,T}} < 1 \ . \tag{13}$$

By introducing the stiffness matrix corresponding to $(\phi_1, \phi_2, \phi_3, \psi_1, ..., \psi_7)$, which has a block structure

$$M = \begin{bmatrix} A & B \\ B^T & C \end{bmatrix}, \quad \text{one obtains}$$

$$\gamma = \sup_{\underline{u}\in\mathbb{R}^3} \sup_{\underline{v}\in\mathbb{R}^7} \frac{\underline{u}^T B \underline{v}}{\sqrt{\underline{u}^T A \underline{u}}\sqrt{\underline{v}^T C \underline{v}}} \ . \tag{14}$$

Therefore, γ is given by the square root of the largest eigenvalue of the generalized eigenproblem

$$(BC^{-1}B^T)\vec{v} = \lambda A\vec{v} \ . \tag{15}$$

Our aim is to express this largest eigenvalue in terms of the angles α and β (see Fig. 1 and note that we can get rid of $\theta = \pi - \alpha - \beta$). The first step in our proof is to reduce (15) into a simpler equation. We have (see [27])

$$A = 2\begin{bmatrix} c+a & -a & -c \\ -a & a+b & -b \\ -c & -b & b+c \end{bmatrix}, \quad B = \frac{1}{3}\left[A|A|0\right], \quad C = \begin{bmatrix} \zeta I & R & u_1 \\ R^T & \zeta I & u_2 \\ u_1^T & u_2^T & 2\zeta \end{bmatrix}$$

where $a := \cot\alpha$, $b := \cot\beta$, $c := \cot\theta$, $\zeta := a+b+c$, I is the identity matrix of order 3, and

$$R = \begin{bmatrix} -b/2 & -a & 0 \\ 0 & -c/2 & -b \\ -c & 0 & -a/2 \end{bmatrix}, \quad u_1 = \begin{bmatrix} -c \\ -a \\ -b \end{bmatrix}, \quad u_2 = \begin{bmatrix} -a \\ -b \\ -c \end{bmatrix}.$$

Let us define the inverse of the upper left blocks of C by

$$K := \begin{bmatrix} \zeta I & R \\ R^T & \zeta I \end{bmatrix}^{-1} \quad \text{which is also given by} \tag{16}$$

$$K = \begin{bmatrix} (\zeta I - (1/\zeta)RR^T)^{-1} & (-1/\zeta)R(\zeta I - (1/\zeta)R^TR)^{-1} \\ (-1/\zeta)R^T(\zeta I - (1/\zeta)RR^T)^{-1} & (\zeta I - (1/\zeta)R^TR)^{-1} \end{bmatrix}. \tag{17}$$

The inverse matrix C^{-1} can also be expressed as

$$C^{-1} = \begin{bmatrix} K + \mu KUU^TK & -\mu KU \\ -\mu U^TK & \mu \end{bmatrix} \text{ with } U := \begin{bmatrix} u_1 \\ u_2 \end{bmatrix}, \quad \mu := \frac{1}{2\zeta - U^TKU}.$$

Because K is given in block structure, $K + \mu KUU^TK$ can also be written block-wise:

$$K + \mu KUU^TK =: \begin{bmatrix} P & Q \\ S & T \end{bmatrix}.$$

The left hand side of (15) becomes therefore

$$\frac{1}{9}[A^T|A^T] \begin{bmatrix} P & Q \\ S & T \end{bmatrix} \begin{bmatrix} A \\ A \end{bmatrix}.$$

As a consequence, the eigenproblem (15) is reduced into:

$$\frac{1}{9}A(P+Q+S+T)\vec{w} = \lambda\vec{w}\,. \tag{18}$$

With the help of (17), we can express P, Q, S and T in terms of α and β. A simple (but long) computations yield that the three eigenvalues of (18) are:

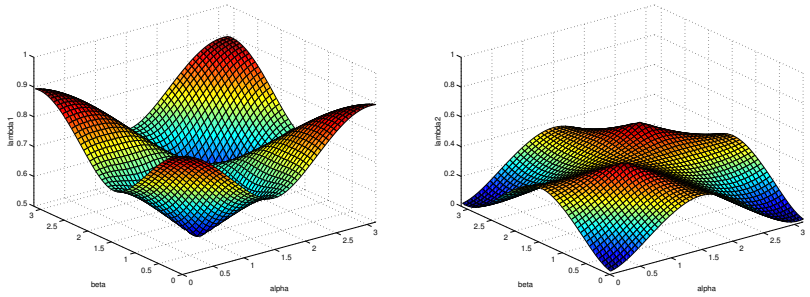

(a) (b)

Fig. 2. Plots of $\lambda_1(\alpha,\beta)$ and $\lambda_2(\alpha,\beta)$

$$\lambda_1 = \lambda_1(\alpha,\beta) = \frac{-2}{D}(-35 + 17c_{42} - \sqrt{d}c_{44} - \sqrt{d}c_{55}s + 34c_{33}s + \sqrt{d}c_{66} - 52c_{11}s + 17c_{24} + 35c_{22} - 34c_{44}), \tag{19}$$

$$\lambda_2 = \lambda_2(\alpha,\beta) = \frac{-2}{D}(-35 + 17c_{42} + \sqrt{d}c_{44} + \sqrt{d}c_{55}s + 34c_{33}s - \sqrt{d}c_{66} - 52c_{11}s + 17c_{24} + 35c_{22} - 34c_{44}), \tag{20}$$

$$\lambda_3 = 0\ , \quad \text{where} \tag{21}$$

$$\begin{aligned}
c_{ij} &:= \cos^i\alpha\cos^j\beta,\\
s &:= \sin\alpha\sin\beta,\\
D &:= -13c_{42} + 138 + 4c_{55}s - 95c_{33}s + 7c_{35}s + 7c_{53}s - 2c_{51}s + \\
&\quad 20c_{02} - 20c_{04} - 2c_{15}s - 38c_{31}s - 38c_{13}s + 238c_{11}s - 20c_{40} + \\
&\quad 20c_{20} - 13c_{24} + 6c_{26} - 4c_{66} - 5c_{64} + 6c_{62} - 211c_{22} + 101c_{44} - 5c_{46},\\
d &:= (121 - 185c_{42} - 32c_{55}s + 182c_{33}s - 56c_{35}s - 56c_{53}s + 16c_{51}s - \\
&\quad 160c_{02} + 160c_{04} + 16c_{15}s + 304c_{31}s + 304c_{13}s - 714c_{11}s + 160c_{40} - \\
&\quad 160c_{20} - 185c_{24} - 48c_{26} + 32c_{66} + 40c_{64} - 48c_{62} + 787c_{22} - 230c_{44} + \\
&\quad 40c_{46})/c_{88}.
\end{aligned}$$

Since λ_1 and λ_2 are functions of (α,β), it is very easy to compute the maximum taken value. For $(\alpha,\beta) \in (0,\pi)\times(0,\pi)$, it can be shown (see Fig. 2(a) and 2(b)) that

$$\max(\lambda_1,\lambda_2) \le \frac{8}{9} \approx 0.888... \tag{22}$$

The theorem is then proved with $\gamma = \frac{2}{3}\sqrt{2}$. □

Remark 5 *The proof was simple but lengthy, a computation supported by MAPLE was helpful in performing all the elementary calculus. The maximum*

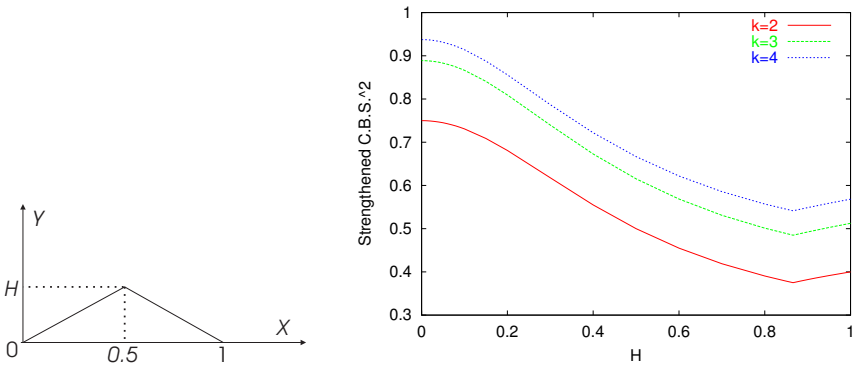

(a) (b)

Fig. 3. (a)The investigated triangle; (b)Strengthened Cauchy-Schwarz constant

value of (22) is approached when one of the angles is tending to π *(see Fig. 2(a) and 2(b)). The result seems to be true for any* $k \geq 2$ *with*

$$\gamma^2 = \frac{k^2 - 1}{k^2} \ ,$$

as the following numerical results show. Readers are refered to [11,8,18] for some ways to determine numerically the strengthened Cauchy-Schwarz constant. The test consists of varying the value of the parameter H *(see Fig. 3(a)) and compute the corresponding strengthened Cauchy-Schwarz constant. The results of the tests are presented in Figure 3(b). One can clearly see that when the triangle becomes anisotropic (*H *tends to* 0*), the strengthened Cauchy-Schwarz Constant is tending to:*

$$\gamma^2 = 0.75 \quad \textit{for } k = 2,$$
$$\gamma^2 = 0.888... \ \textit{for } k = 3,$$
$$\gamma^2 = 0.9375 \ \textit{for } k = 4.$$

The smallest value of the Cauchy-Schwarz constant is obtained for $H = 0.8660254$ *where the triangle is equilateral. It is however worth noting that* $k \geq 4$ *is not of any interest because that leads to overly many nodes for each element and that results in too intensive computational costs for the a-posteriori error estimator.*

Before we state a corollary of Theorem 4, let us introduce the following space

$$Z_h := \{\vec{v} \in L_2(\Omega)^2 : \vec{v}|_T \in Z(T)^2 \quad \forall T \in \mathbf{T}_h\} \, . \tag{23}$$

Corollary 6 (Strengthened Cauchy-Schwarz inequality) Let $\mathbf{T}_h$ be a mesh (anisotropic or not). For V_h and Z_h defined in (5) and (23), there is exists $\gamma \in [0,1)$ which is independent of any property of $\mathbf{T}_h$ such that

$$\langle \vec{v}, \vec{z} \rangle \leq \gamma |||\vec{v}|||.|||\vec{z}||| \quad \forall \vec{v} \in V_h, \ \forall \vec{z} \in Z_h. \tag{24}$$

PROOF.

Let $\vec{v} = (v_1, v_2)$ and $\vec{z} = (z_1, z_2)$ be in V_h and Z_h respectively.

By definition (10) we have

$$\langle \vec{v}, \vec{z} \rangle = \sum_{T \in \mathbf{T}_h} \langle v_1, z_1 \rangle_T + \langle v_2, z_2 \rangle_T.$$

Therefore, according to Theorem 4, we obtain

$$\langle \vec{v}, \vec{z} \rangle \leq \gamma \sum_{T \in \mathbf{T}_h} \left\{ |v_1|_{1,T} |z_1|_{1,T} + |v_2|_{1,T} |z_2|_{1,T} \right\}.$$

From the usual Cauchy-Schwarz inequality we deduce

$$\langle \vec{v}, \vec{z} \rangle \leq \gamma \left\{ \sum_{T \in \mathbf{T}_h} |v_1|^2_{1,T} + |v_2|^2_{1,T} \right\}^{1/2} \left\{ \sum_{T \in \mathbf{T}_h} |z_1|^2_{1,T} + |z_2|^2_{1,T} \right\}^{1/2}.$$

□

4 A-posteriori error estimator

Definition 7 For each element $T \in \mathbf{T}_h$, let $\vec{e}_T = (e_T^1, e_T^2) \in Z(T)^2$ be the solution of the Poisson problem:

$$a_T(\vec{e}_T, \vec{v}) = (\vec{f}, \vec{v})_T - a_T(\vec{u}_T, \vec{v}) \quad \forall\, \vec{v} \in Z(T)^2\,, \tag{25}$$

where $\vec{u}_T$ is the restriction of the solution $\vec{u}_h$ of problem (7) in the element T. We define the following expression which will be the a-posteriori error estimator.

$$\eta_T := \sqrt{|e_T^1|^2_{1,T} + |e_T^2|^2_{1,T}}\,. \tag{26}$$

Before we can prove the equivalence of this a-posteriori error estimator to the true error, let us introduce the following definitions.

Definition 8 (Hierarchical space enlargement) For each element $T \in \mathbf{T}_h$, we define the local space

$$R(T) := \{\vec{v} \in H^1(T)^2 : \operatorname{div} \vec{v} = 0\}. \tag{27}$$

We introduce also the global spaces

$$R := \{\vec{v} \in L_2(\Omega)^2 : \vec{v}|_T \in R(T) \quad \forall\, T \in \mathbf{T}_h\}. \tag{28}$$

Now we enlarge the space $V_h \cap R$ hierarchically into W_h:

$$W_h := (V_h \cap R) \oplus Z_h\,, \tag{29}$$

where $\oplus$ stands for direct sum (and not orthogonal sum).

Definition 9 If we approximate the following continuous problem

$$\begin{cases} \text{Find } \vec{E} \in \mathbb{H}^2 \ : \\ a_h(\vec{E}, \vec{v}) = (\vec{f}, \vec{v}) - a_h(\vec{u}_h, \vec{v}) \quad \forall\, \vec{v} \in V \cap R \end{cases} \tag{30}$$

in the finite dimensional spaces V_h and W_h as,

$$\begin{cases} \text{Find } \vec{v}_h \in V_h \ : \\ a_h(\vec{v}_h, \vec{v}) = (\vec{f}, \vec{v}) - a_h(\vec{u}_h, \vec{v}) \quad \forall\, \vec{v} \in V_h \cap R \end{cases} \tag{31}$$

$$\begin{cases} \text{Find } \vec{w}_h \in W_h \ : \\ a_h(\vec{w}_h, \vec{v}) = (\vec{f}, \vec{v}) - a_h(\vec{u}_h, \vec{v}) \quad \forall\, \vec{v} \in W_h, \end{cases} \tag{32}$$

then we say that the saturation assumption is met if

$$\exists\, \beta < 1 : \quad |||\vec{E} - \vec{w}_h||| \leq \beta |||\vec{E} - \vec{v}_h|||. \tag{33}$$

Remark 10 *The saturation assumption (33) quantifies that the solution in the larger space W_h is more accurate than that in the smaller space V_h (See [28,16] for further investigation of this assumption). Note that problems (30), (31), (32) were only defined in order to introduce the saturation assumption. We do not need to solve any of them in practice. In the last section of this*

paper, we will show numerical evidence of how to achieve this assumption in practice.

Theorem 11 If we suppose that the saturation assumption (33) is fulfilled then there exist two constants $\underline{C}$ and $\overline{C}$ which are independent of h and the aspect ratio σ_h of the mesh $\mathbf{T}_h$ such that

$$\underline{C} \sum_{T\in\mathbf{T}_h} \eta_T^2 \leq |||\vec{E}|||^2 \leq \overline{C} \sum_{T\in\mathbf{T}_h} \eta_T^2. \tag{34}$$

Remark 12 *A theorem similar to this has been discussed in [22,1] where the authors have used extensively the shape regularity of the mesh.*

PROOF.

Part 1 (Efficiency):

Let us define $\vec{E}_h \in Z_h$ by

$$\vec{E}_h|_T := \vec{e}_T \quad \forall\, T \in \mathbf{T}_h \tag{35}$$

We note immediately that $\vec{E}_h$ is the solution of:

$$a_h(\vec{E}_h, \vec{v}) = (\vec{f}, \vec{v}) - a_h(\vec{u}_h, \vec{v}) \qquad \forall\, \vec{v} \in Z_h \tag{36}$$

because equation (25) implies:

$$\sum_{T\in\mathbf{T}_h} a_T(\vec{e}_T, \vec{v}) = \sum_{T\in\mathbf{T}_h} \left[(\vec{f}, \vec{v})_T - a_T(\vec{u}_T, \vec{v})\right] .$$

Therefore, we obtain:

$$\left[\sum_{T\in\mathbf{T}_h} \eta_T^2\right]^{1/2} = |||\vec{E}_h||| \leq \sup_{\substack{\vec{z}\in Z_h \\ |||\vec{z}|||=1}} a_h(\vec{E}_h, \vec{z}) = \sup_{\substack{\vec{z}\in Z_h \\ |||\vec{z}|||=1}} a_h(\vec{w}_h, \vec{z}) \tag{37}$$

$$\leq \sup_{\substack{\vec{z}\in Z_h \\ |||\vec{z}|||=1}} |||\vec{w}_h|||.|||\vec{z}||| = |||\vec{w}_h|||. \tag{38}$$

We have the second equality in (37) because the right hand sides of (32) and (36) coincide for all $\vec{z} \in Z_h \subset W_h$.

On the other hand, we obtain from (33) that

$$|||\vec{w}_h||| \leq |||\vec{E} - \vec{w}_h||| + |||\vec{E}||| \leq \beta|||\vec{E}||| + |||\vec{E}||| = (1+\beta)|||\vec{E}||| \ , \tag{39}$$

whereby used the fact that $\vec{v}_h$ of (31) is the zero function because $a_h(\vec{u}_h, \vec{v}) = (\vec{f}, \vec{v})$ for all function $\vec{v}$ which is divergence free (see problem (7)).

This last inequality and (38) yield:

$$\left[\sum_{T\in\mathbf{T}_h} \eta_T^2\right]^{1/2} \leq (1+\beta)\,|||\vec{E}|||. \tag{40}$$

Part 2 (Reliability):

Let $\vec{v} \in V_h \cap R$ and $\vec{z} \in Z_h$ be such that $|||\vec{v}+\vec{z}||| = 1$. Then

$$\begin{aligned} 1 &= |||\vec{v}+\vec{z}|||^2 = |||\vec{v}|||^2 + |||\vec{z}|||^2 + 2\langle \vec{v}, \vec{z}\rangle && (41)\\ &\geq |||\vec{v}|||^2 + |||\vec{z}|||^2 - 2\gamma |||\vec{v}|||.|||\vec{z}||| && (42)\\ &= (|||\vec{v}|||^2 - \gamma|||\vec{z}|||)^2 + (1-\gamma^2)|||\vec{z}|||^2 && (43)\end{aligned}$$

Consequently,

$$1 \geq (1-\gamma^2)|||\vec{z}|||^2\,. \tag{44}$$

We have on the other hand:

$$|||\vec{E}||| \leq |||\vec{E} - \vec{w}_h||| + |||\vec{w}_h||| \leq \beta|||\vec{E}||| + |||\vec{w}_h|||\,,$$

(we used again the same technique as in (39)) which implies:

$$(1-\beta)|||\vec{E}||| \leq |||\vec{w}_h|||\,. \tag{45}$$

Now, we use (44) to obtain

$$\begin{aligned} |||\vec{w}_h||| &\leq \sup_{\substack{|||\vec{v}+\vec{z}|||=1\\ (\vec{v},\vec{z})\in(V_h\cap R)\times Z_h}} a_h(\vec{w}_h, \vec{v}+\vec{z}) && (46)\\ &= \sup_{\substack{|||\vec{v}+\vec{z}|||=1\\ (\vec{v},\vec{z})\in(V_h\cap R)\times Z_h}} (\vec{f}, \vec{v}+\vec{z}) - a_h(\vec{u}_h, \vec{v}+\vec{z}) && (47)\\ &= \sup_{\substack{|||\vec{v}+\vec{z}|||=1\\ (\vec{v},\vec{z})\in(V_h\cap R)\times Z_h}} \underbrace{(\vec{f}, \vec{v}) - a_h(\vec{u}_h, \vec{v})}_{=0} + \underbrace{(\vec{f}, \vec{z}) - a_h(\vec{u}_h, \vec{z})}_{a_h(\vec{E}_h, \vec{z})} \\ &\leq \frac{1}{\sqrt{1-\gamma^2}}|||\vec{E}_h||| = \frac{1}{\sqrt{1-\gamma^2}}\left[\sum_{T\in\mathbf{T}_h} \eta_T^2\right]^{1/2}. && (48)\end{aligned}$$

According to (45) and this last inequality,

$$|||\vec{E}||| \leq \frac{1}{1-\beta}|||\vec{w}_h||| \leq \frac{1}{(1-\beta)\sqrt{1-\gamma^2}} \left[\sum_{T\in\mathbf{T}_h} \eta_T^2\right]^{1/2} .$$

Finally, the theorem is proved and:

$$\frac{1}{(1+\beta)^2} \sum_{T\in\mathbf{T}_h} \eta_T^2 \leq |||\vec{E}|||^2 \leq \frac{1}{(1-\beta)^2(1-\gamma^2)} \sum_{T\in\mathbf{T}_h} \eta_T^2 . \tag{49}$$

□

5 Numerical results

The purpose of this section is to show the numerical performance of our a-posteriori error estimator. To that end, we consider four test problems: an internal layer, a boundary layer, a re-entrant corner and a crack problem. We will always start from a coarse mesh which will then be further refined adaptively. Before discussing the test problems, we want to describe our mesh refinement approach.

5.1 Mesh operations and anisotropy direction:

In the course of the mesh refinement, we distinguish three mesh operations:

(Op1) Subdivision of a triangle T into three sub-triangles by joining the center of gravity and the three apices (See Fig. 4(a)). This will be used to subdivide a triangle T for which η_T is too large.

(Op2) Edge flipping (See Fig. 4(b)). This can only be applied if the union of the two incident triangles form a convex set.

(Op3) Subdivision of a triangle T into two sub-triangles (See Fig. 4(c)). This will only be applied to a boundary element by joining the middle of the boundary edge and the internal node.

Definition 13 Suppose $\vec{u} = (u_{h1}, u_{h2})$, and p_h are the solution on the current mesh. Let (x, y) be the middle of an edge e. Consider some elements T_{s_k} in the proximity of e and approximate u_{h1} (resp. u_{h2} , resp. p_h) by a single (i.e. non-piecewise) polynomial Q_1 (resp. Q_2 , resp. Q_p) (See [21]) inside $F := \cup_k T_{s_k}$. Introduce

$$\vec{F}_i(x, y) := [x, y, Q_i(x, y)] \qquad i = 1, 2, p.$$

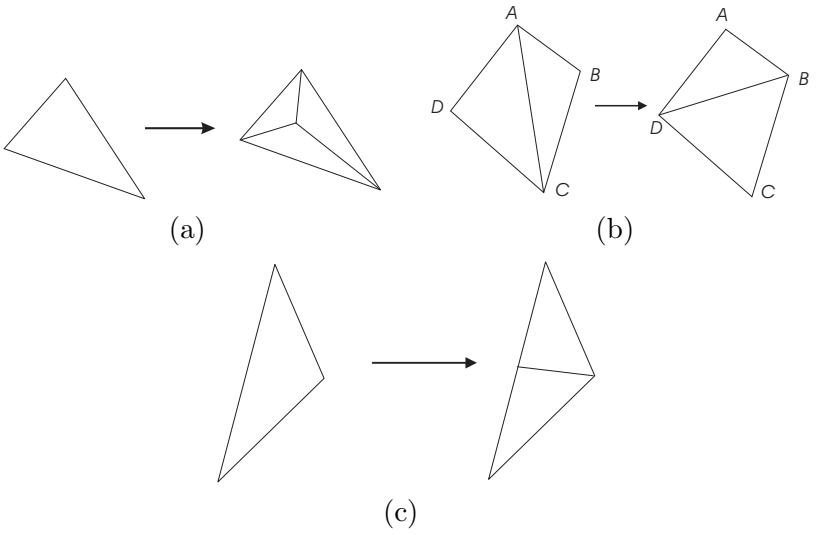

Fig. 4. (a)Subdivision (b)Edge flipping (c)Boundary refinement

The corresponding normal vectors are therefore

$$\vec{n}_i(x,y) = \frac{\partial \vec{F}_i}{\partial x} \times \frac{\partial \vec{F}_i}{\partial y} \qquad i = 1, 2, p. \tag{50}$$

We define now $\vec{N}(x,y) := \vec{n}_1(x,y) + \vec{n}_2(x,y) + \vec{n}_p(x,y) \in \mathbb{R}^3$. Let $\vec{m}(x,y) \in \mathbb{R}^2$ denote the first two components of $\vec{N}(x,y)$ and $\vec{t}(x,y) \in \mathbb{R}^2$ be a perpendicular vector to $\vec{m}(x,y)$. With E being the set of all edge midpoints, we define finally the anisotropy direction to be

$$\vec{\tau}(x,y) := \frac{\vec{t}(x,y)}{t_{\max}} \qquad \text{where} \quad t_{\max} := \max_{(x,y)\in E} |\vec{t}(x,y)|.$$

As an illustration, in Fig. 5(b) and Fig. 6(b) the fields $\vec{\tau}(x,y)$ follow the layer orientations. In Fig. 7(b) and Fig. 8(b) they do not follow any special direction.

5.2 Anisotropic mesh refinement algorithm

We start from a mesh $\mathbf{T}_{h,0}$ which is both coarse and isotropic. We will now describe the way to deduce $\mathbf{T}_{h,k+1}$ from $\mathbf{T}_{h,k}$. First, we compute all a-posteriori errors η_T of formula (25) and (26) corresponding to $T \in \mathbf{T}_{h,k}$. We subdivide the elements (say 12 percent) which have the largest error by applying mesh operation (Op1).

As a second step, we consider every edge e and its midpoint (x,y) and we compute the value of $\vec{\tau}(x,y)$. By choosing a threshold value $\delta \in [0,1]$, we can distinguish two cases according to the value of $|\vec{\tau}(x,y)|$ with respect to δ.

If $|\vec{\tau}(x,y)| \in [0,\delta)$, we perform the usual Delaunay edge flipping (see [10],[19]) to e. In the case $|\vec{\tau}(x,y)| \in [\delta,1]$, we apply the technique of generalized Voronoi triangulation (see [26], [12]) which we want to describe briefly now. Denote by A, B, C, D the apices of the incident triangles to the edge e (see Fig. 4(b)). If the following generalized swapping criterion is satisfied then we flip the edge e.

$$\begin{aligned} &\|(C- B) \times (A-B)\|(A-D)^T \mathbf{M}_{(x,y)}(C-D)+ \\ &\qquad (C-B)^T \mathbf{M}_{(x,y)}(A-B)\|(A-D) \times (C-D)\| < 0 \quad \text{where} \end{aligned} \tag{51}$$

$$\mathbf{M}_{(x,y)} = \begin{bmatrix} \cos\theta & -\sin\theta \\ \sin\theta & \cos\theta \end{bmatrix} \begin{bmatrix} 1/r_1^2 & 0 \\ 0 & 1/r_2^2 \end{bmatrix} \begin{bmatrix} \cos\theta & \sin\theta \\ -\sin\theta & \cos\theta \end{bmatrix}. \tag{52}$$

In the last equations, θ denotes the polar angle of $\vec{\tau}(x,y)$, r_2 is any positive number and by choosing a large parameter χ,

$$r_1 := \lambda r_2 \chi + (1-\lambda) r_2 \quad \text{where} \quad \lambda := \frac{|\vec{\tau}(x,y)| - \delta}{1-\delta} \in [0,1]. \tag{53}$$

As for boundary elements $T \in \mathbf{T}_{h,k}$, if the longest edge e is the boundary one and if e is not in the same orientation as $\vec{\tau}(x,y)$, we apply mesh operation (Op3) to T. The advantage of those mesh operations over some others is that they induce no hanging node whatsoever. Therefore every mesh manipulation can be kept local in the implementational point of view.

5.3 Internal layer

We want to investigate an internal layer problem on a domain Ω which is supposed to be the unit square $[0,1]^2$. The exact solution of the velocity is

$$\vec{u}(x,y) := \begin{bmatrix} 10x^2(x-1)^2 y(y-1)(2y-1) \\ 10y^2(y-1)^2 x(x-1)(2x-1) \end{bmatrix}. \tag{54}$$

The pressure $p(x,y)$ is chosen to have an internal layer (see Fig. 5(e)) along the curve $y = \alpha(x)$ with

$$\alpha(x) = 10.4794x^5 - 23.6686x^4 + 15.3989x^3 - 1.9598x^2 + 0.3500. \tag{55}$$

That has been done in the following fashion. Consider the univariate function $L(t) := \sin[sign(t)|0.5\pi t|^s]$ which presents a layer at $t = 0$ if s is small in size.

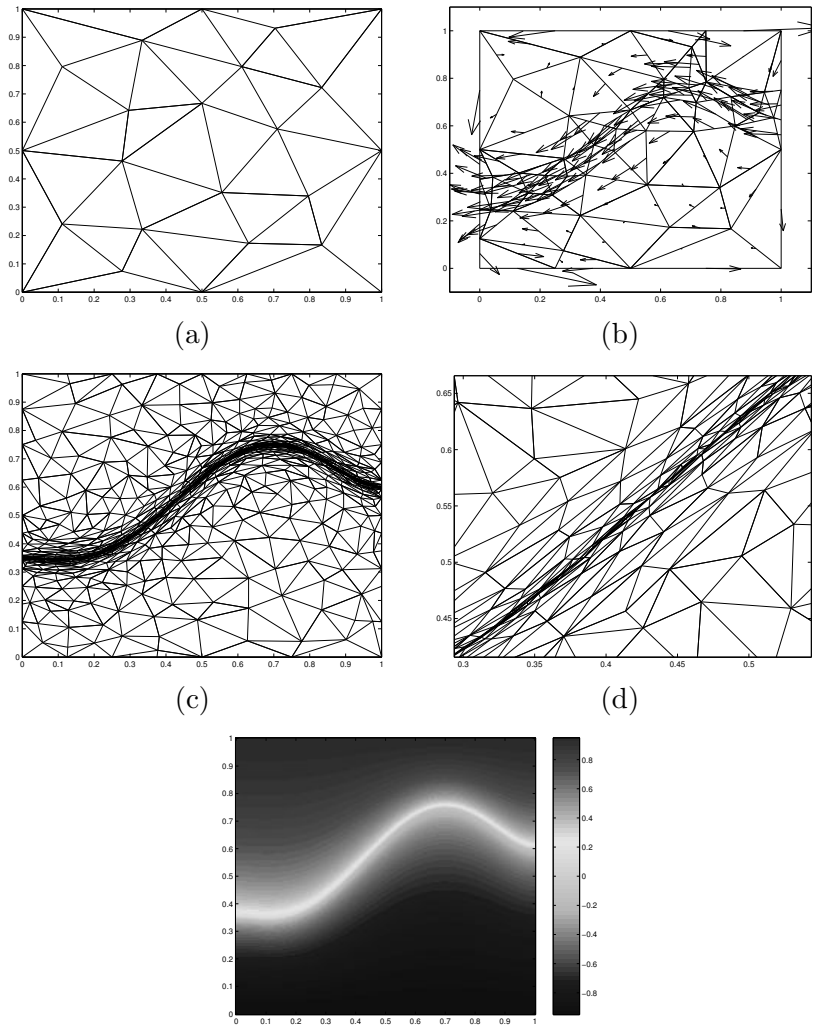

Fig. 5. (a)Coarse mesh for the internal layer problem (b)$\vec{\tau}(x, y)$ field; (c)Finest mesh; (d)Zoom in $[0.3, 0.55] \times [0.4, 0.65]$; (e)Exact solution of internal layer;

Table 1
Internal layer: ratio between exact error and a-posteriori error

nb. elements	Aspect ratio	error ratio	effeciency
38	7.51 E+000	1.027830	1.027830
151	1.82 E+002	1.001999	1.001999
191	8.13 E+003	1.033813	1.033813
387	2.25 E+004	0.970307	1.030602
796	2.25 E+004	1.078548	1.078548
1266	2.25 E+004	1.070143	1.070143

As the value of s tends to zero, the width of the layer becomes thinner. For $(x, y) \in [0, 1]^2$, we define the exact pressure to be

$$p(x,y) := \begin{cases} L\left[(y - \alpha(x))/\alpha(x)\right] + K & \text{if } \ y < \alpha(x) \\ L\left[(y - \alpha(x))/(1 - \alpha(x))\right] + K & \text{if } y \geq \alpha(x). \end{cases}$$

The constant K is determined so that the pressure has zero integral. The initial mesh (Fig. 5(a)) for this internal layer problem consists of 38 isotropic triangles. In Fig. 5(c), we find the final mesh which has 1715 elements. The mesh is obviously dense in the vicinity of the internal layer. The closeup in Fig. 5(d) shows that the elements are also thin and stretched along the layer orientation and it is isotropic elsewhere.

5.4 Boundary layer

We want now to study a boundary layer problem in which the domain Ω is again the unit square. The exact solutions are chosen to be:

$$\vec{u}(x,y) := \left[(\mu - 1)y^{\mu-1}/\mu, (\mu - 1)x^{\mu-1}/\mu\right] \tag{56}$$

$$p(x,y) := (x - 0.5)(y - 0.5). \tag{57}$$

The velocity presents a boundary layer at the right and the upper boundaries. The width of the layer is controlled by the parameter μ in the equation (56). As μ increases in size, the boundary layer becomes thinner. We start from the same initial mesh as in the former problem. In Fig. 6(c) we find the final mesh having 3265 elements. As we approach the position of the boundary layer, the mesh becomes both dense and anisotropic as is demonstrated in Fig. 6(d).

Table 2
Boundary layer: ratio between exact error and a-posteriori error

nb. elements	Aspect ratio	error ratio	efficiency
38	7.51 E+000	1.191296	1.191296
53	1.13 E+001	1.309279	1.309279
282	5.81 E+002	0.906400	1.103265
744	5.95 E+003	0.906323	1.103360
1490	7.14 E+003	1.145491	1.145491

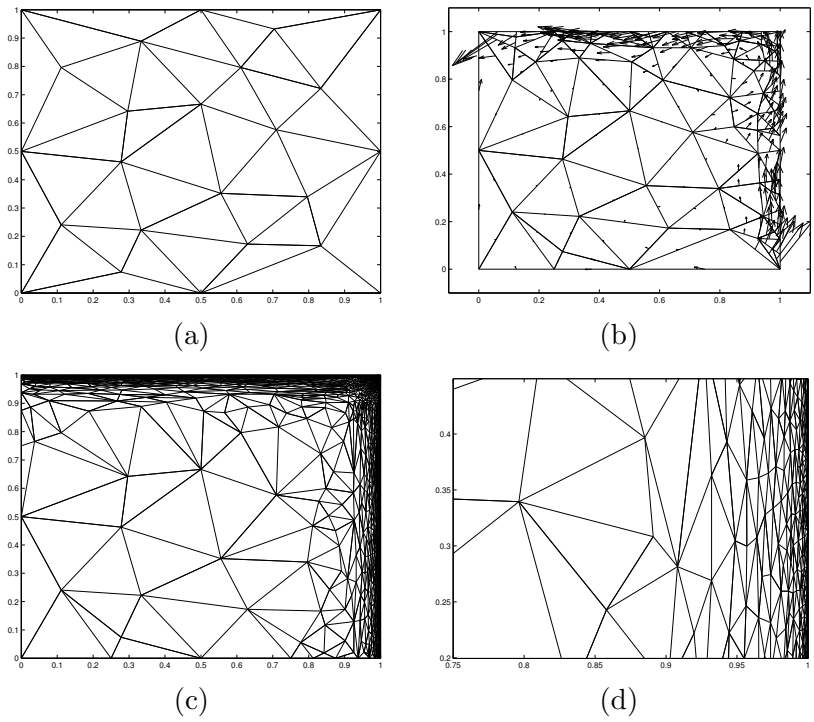

Fig. 6. (a)Coarse mesh for the boundary layer problem; (b)$\vec{r}(x,y)$ field; (c)Finest mesh; (d)Zoom inside $[0.75,1]\times[0.2,0.45]$

5.5 Re-entrant corner

In this third test we perform our test on the domain

$$\Omega=\left\{(x,y)\in\mathbb{R}^2 : x^2+y^2<1 \text{ and } (x,y)\notin[0,\infty)\times(-\infty,0]\right\}. \qquad (58)$$

We take the exact solutions from [33,34]. Their expressions in polar variables (r,θ) are as follows.

Table 3
Re-entrant corner: ratio between exact error and a-posteriori error

nb. elements	Aspect ratio	error ratio	efficiency
14	2.84	1.032237	1.032237
236	5.81	1.110648	1.110648
481	7.04	1.108649	1.108649
967	16.7	1.058267	1.058267
1217	25.1	0.841642	1.188153
1540	37.4	0.971552	1.029287

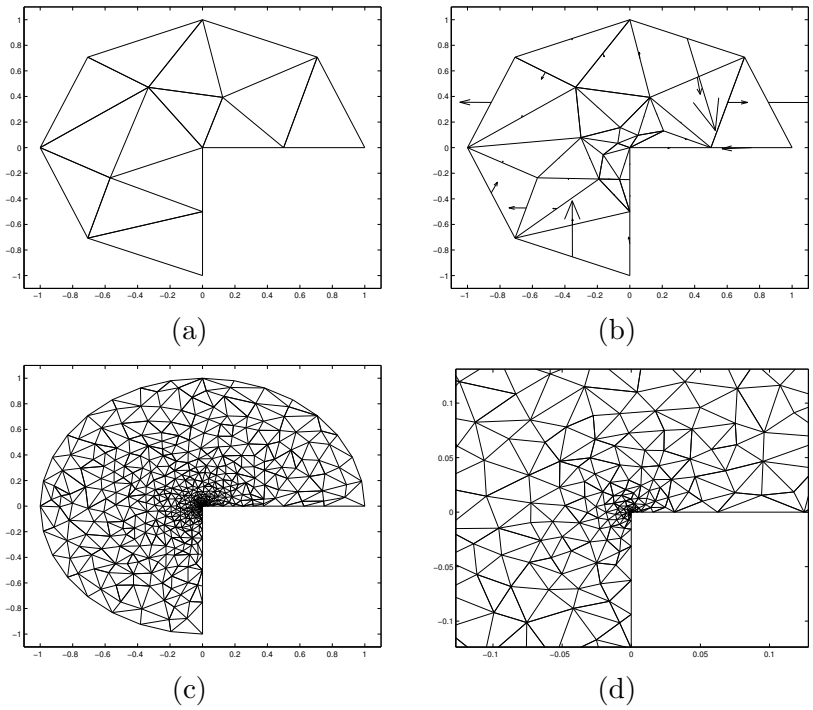

Fig. 7. (a)Coarse mesh for the re-entrant; (b)$\vec{\tau}(x,y)$ field; (c)Finest mesh; (d)Zoom inside $[-0.15, 0.15] \times [-0.15, 0.15]$

$$\zeta(\theta) := \sin((1+\alpha)\theta)\cos(1.5\pi\alpha)/(1+\alpha) - \cos((1+\alpha)\theta) \tag{59}$$

$$+ \sin((\alpha-1)\theta)\cos(1.5\pi\alpha)/(1-\alpha) - \cos((\alpha-1)\theta) \tag{60}$$

$$\psi(r,\theta) := r^{1+\alpha}\zeta(\theta) \tag{61}$$

$$\vec{u} := \left[\frac{\partial\psi}{\partial y}\,,\ -\frac{\partial\psi}{\partial x}\right] \tag{62}$$

$$p(x,y) := \frac{-r^{\alpha-1}}{1-\alpha}\left[(1+\alpha)^2\partial_\theta\zeta(\theta) + \partial_\theta^3\zeta(\theta)\right], \tag{63}$$

where $\alpha := 856399/1572864$. The initial mesh is very isotropic and has only 14 elements (see Fig. 7(a)). The final mesh (See Fig. 7(c)) has 967 elements and it does not present any special anisotropy direction. The closeup in Fig. 7(d) shows that the density of the mesh is very high in the neighborhood of the re-entrant corner.

5.6 Crack

Our last test deals with the investigation of a crack problem in which the domain of study is

$$\Omega = \left\{(x,y) \in \mathbb{R}^2 : x^2 + y^2 < 1 \ \text{ and } \ (x,y) \notin [0,\infty) \times \{0\}\right\}. \tag{64}$$

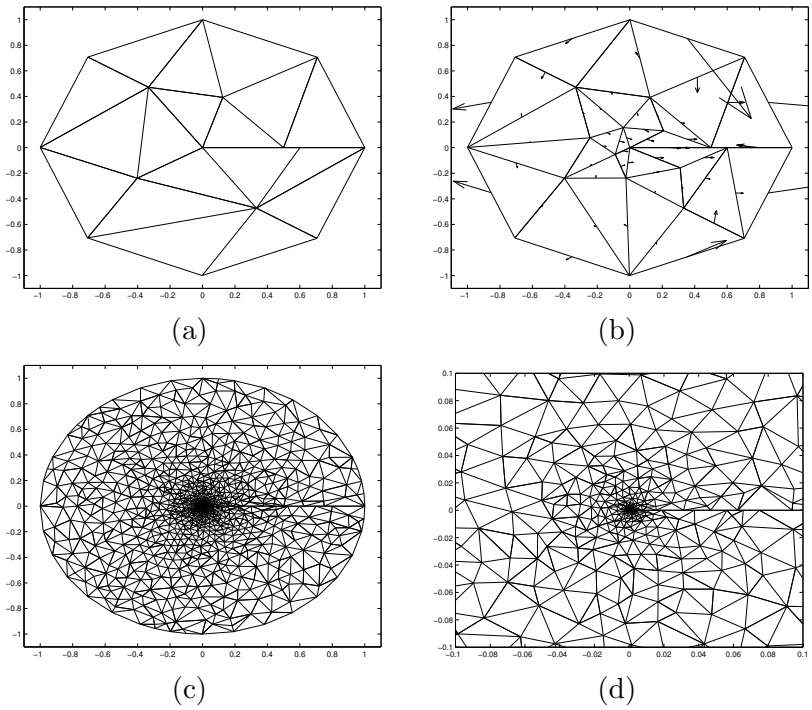

Fig. 8. (a)Coarse mesh for the crack problem; (b)$\vec{\tau}(x, y)$ field; (c)Finest mesh; (d)Zoom inside $[-0.1, 0.1] \times [-0.1, 0.1]$

The exact solutions are again those in [33,34] which are given in polar coordinates by:

$$\zeta(\theta) := 3\sin(0.5\,\theta) - \sin(1.5\,\theta) \tag{65}$$

$$\psi(r, \theta) := r^{1.5}\zeta(\theta) \tag{66}$$

$$\vec{u} := \left[\frac{\partial \psi}{\partial y}\,,\ -\frac{\partial \psi}{\partial x}\right] \tag{67}$$

$$p(x, y) := \frac{-2}{\sqrt{r}}\left[2.25\partial_\theta \zeta(\theta) + \partial_\theta^3 \zeta(\theta)\right]. \tag{68}$$

The refinement history of the crack problem behaves in the same manner as that of the re-entrant corner. Starting from an isotropic mesh with 18 elements (see Fig. 8(a)), we end with an isotropic mesh having 1946 elements (see Fig. 8(c)). The mesh density at the origin is illustrated in the Fig. 8(d).

5.7 Saturation assumption, anisotropy and error ratio

The value of the parameter χ in equation (53) controls the anisotropy of the mesh. By choosing a very large χ (say 10^4), we allow the aspect ratio to become very large without letting it tend to infinity. That is already mentioned in [26,12] because the ratio r_1/r_2 which reflects the anisotropy of the mesh

Table 4
Crack problem: ratio between exact error and a-posteriori error

nb. elements	Aspect ratio	error ratio	efficiency
18	3.81	1.519440	1.519440
110	6.89	1.519440	1.519440
373	7.51	1.165327	1.165327
760	7.51	1.155433	1.155433
1504	8.26	1.135096	1.135096
2387	8.62	1.153799	1.153799

resides in the interval $[1, \chi]$.

In other words, by using the mesh refinement in section 5.2, triangles might become highly anisotropic without being degenerated. The saturation assumption is known to be valid (see [1]) in our case where the aspect ratio is not tending to infinity. For the four previous tests we have computed the ratio between the exact error and the a-posteriori error:

$$R := \frac{|||\vec{u}_{\text{err}}|||^2 + \|p_{\text{err}}\|_0^2}{\sum_{T \in \mathbf{T}_h} \eta_T^2}.$$

We gather in the last four tables the relationship between the number of elements, the largest aspect ratio, the error ratio R, and the efficiency which we define by $\max(R, 1/R) \in [1, \infty)$. From equation (49), we deduce that the error ratio R is bounded above by $C/(1-\beta)^2$. That is, if the error ratio is very large then $C/(1-\beta)^2$ tends to infinity or equivalently β becomes very close to unity. In all tests, we see that the error ratio is bounded. We remark from Table 1 and Table 2 that escalation of the aspect ratio does not affect the efficiency of the error estimator. For example, in the case of boundary layer, the error ratio for an aspect ratio of 7.51 is comparable to that for an aspect ratio of 7.14×10^3. The sensitivity of the a-posteriori error estimator is not influenced by the size of the aspect ratio.

6 Acknowledgment

The author wishes to thank Prof. Dr. Th. Apel for helping him during the conception of this paper.

References

[1] B. Achchab, A. Agouzal, J. Baranger and J.F. Maitre, Estimateur d'erreur a posteriori hiérarchique. Application aux éléments finis mixtes, *Numer. Math.*, **80** (1998) pp. 159-179.

[2] G. Acosta and R. G. Durán, The maximum angle condition for mixed and non-conforming elements. Application to the Stokes equations, *SIAM J. Numer. Anal.* **37** (1999) pp. 18-36.

[3] M. Ainsworth and T. Oden, A Posteriori error estimators for the Stokes and Oseen equations, *SIAM J. Numer. Anal.* **34** (1997) pp. 228-245.

[4] T. Apel, *Anisotropic Finite Elements: Local estimates and applications, Teubner*, Stuttgart, 1999.

[5] T. Apel and S. Nicaise and J. Schöberl, A non-conforming finite element method with anisotropic mesh grading for the Stokes problem in domains with edges, *IMA J. Numer. Anal.* **21** No. 4 (2001) pp. 843-856.

[6] T. Apel and S. Nicaise and J. Schöberl, Crouzeix-Raviart type finite elements on anisotropic meshes, *Numer. Math.* **89** No. 2 (2001) pp. 193-223.

[7] T. Apel and M. Randrianarivony, Stability of discretizations of the Stokes problem on anisotropic meshes, *Math. Comput. Simul.* **3-6** (2003) pp. 437-447.

[8] R. Bank, Hierarchical bases and the finite element method, *Acta Numerica* 1996, pp. 1-43.

[9] R. Becker and R. Rannacher, Finite element solution of the incompressible Navier-Stokes equations on anisotropically refined meshes, Proceedings of the tenth GAMM-Seminar, Kiel, Germany, January 1994. *Notes Numer. Fluid Mech.* **49** (1995) pp. 52-62.

[10] M. de Berg, M. van Kreveld, M. Overmars and O. Schwarzkopf, *Computational Geometry, Springer*, Berlin, 1997.

[11] A. Björck and G. Golub, Numerical methods for computing angles between linear subspaces, *Math. Comp.* **123** (1973) pp. 579-594.

[12] F. Bossen and P. Heckbert, A pliant method for anisotropic mesh generation, in: 5th International Meshing Roundtable: Proceeding, Sandia National Laboratories, October 1996, pp. 63-76.

[13] P. Capon and P. K. Jimack, An adaptive finite element method for the compressible Navier-Stokes equations, in: Numerical methods for fluid dynamics V. Proceedings of the conference, Oxford, UK, April 1995, pp. 327-333.

[14] E. Creusé, G. Kunert and S. Nicaise, A posteriori error estimation for the Stokes problem, Preprint SFB 393 No. 03-01, TU Chemnitz, 2003.

[15] M. Dobrowolski, S. Gräf and C. Pflaum,

A Posteriori error estimators in the finite element method on anisotropic meshes, *ETNA* **8** (1999) pp. 36-45.

[16] W. Dörfler and R. Nochetto, Small data oscillation implies the saturation assumption, *Numer. Math.* **91** No. 1 (2002) pp. 1-12.

[17] V. Dolejsí, Anisotropic mesh adaptation technique for viscous flow simulation, *East-West J. Numer. Math.* **9** No.1 (2001) pp. 1-24.

[18] V. Eijkhout and P. Vassilevski, The role of the Strengthened Cauchy-Buniakowskii-Schwarz inequality in multilevel methods, *SIAM Review* **33** (1991) pp. 405-419.

[19] P. George and H. Borouchaki, *Delaunay triangulation and meshing, Hermes*, Paris, 1998.

[20] V. Girault and P.-A. Raviart, *Finite Element Methods for Navier-Stokes Equations, Springer*, Paris, 1986.

[21] J. Hoschek and D. Lasser, *Grundlagen der geometrischen Datenverarbeitung, Teubner*, Stuttgart, 1989.

[22] J. Jou and J. L. Liu, An a posteriori finite element analysis for the Stokes equations, *J. Comput. Appl. Math.*, **114** (2000) pp. 333-343.

[23] G. Kunert, A posteriori L_2 error estimation on anisotropic tetrahedral finite element meshes, *IMA J. Numer. Anal.*, **21** (2001) pp. 503-523.

[24] G. Kunert, Robust a posteriori error estimation for a singularly perturbed reaction-diffusion equation on anisotropic tetrahedral meshes, Preprint SFB 393 No. 00-39, TU Chemnitz, 2000.

[25] G. Kunert and R. Verfürth, Edge residuals dominate a posteriori error estimates for linear finite element methods on anisotropic triangular and tetrahedral meshes, *Numer. Math.* **86** (2000) pp. 283-303.

[26] F. Labelle and J. Shewchuk, Anisotropic Voronoi diagrams and guaranteed-quality anisotropic mesh generation, *ACM SoCG* (2003) (to appear) (www.cs.berkeley.edu/ flab)

[27] J. F. Maitre and F. Musy, The contraction number of a class of two-level methods; an exact evaluation for some finite element subspaces and model problems, in: Multigrid Methods: Proceedings, Cologne, Vol. 960, 1981, pp. 535-544.

[28] R. Nochetto, Removing the saturation assumption in a posteriori error analysis, in: Istit. Lombardo Accad. Sci. Lett. Rend. A, Vol. 127, 1993, pp. 67-82.

[29] W. Rachowicz, An anisotropic h-adaptive finite element method for compressible Navier-Stokes equations, *Comput. Methods Appl. Mech. Engrg* **146** (1997) pp. 231-252.

[30] M. Randrianarivony, Stability of mixed finite element methods on anisotropic meshes, Master's thesis, Faculty of mathematics, Technische Universität Chemnitz, 2001.

[31] K. Siebert, An a posteriori error estimator for anisotropic refinement, *Numer. Math.* **73** No.3 (1996) pp. 373-398.

[32] S. Shaw and J. Whiteman, Towards adaptive finite element schemes for partial differential Volterra equation solvers, *J. Adv. Comput. Math.* **6** No.3-4 (1996) pp. 309-323.

[33] R. Verfürth, A Posteriori error estimators for the Stokes equations, *Numer. Math.* **55** (1989) pp. 309-325.

[34] R. Verfürth, A Posteriori error estimators for the Stokes equations II: non-conforming discretizations, *Numer. Math.* **60** (1991) pp. 235-249.